

Realism in Action: Anomaly-Aware Diagnosis of Brain Tumors from Medical Images Using YOLOv8 and DeiT

1st Seyed Mohammad Hossein Hashemi

Department of CS & IT
Institute for Advanced Studies in Basic Sciences (IASBS)
Zanjan, Iran
mh.hashemi@iasbs.ac.ir

2nd Leila Safari

Department of Computer Engineering
University of Zanjan (ZNU)
Zanjan, Iran
lsafari@znu.ac.ir

3rd Mohsen Hooshmand

Department of CS & IT
Institute for Advanced Studies in Basic Sciences (IASBS)
Zanjan, Iran
mohsen.hooshmand@iasbs.ac.ir

4th Amirhossein Dadashzadeh Taromi

Department of CS & IT
Institute for Advanced Studies in Basic Sciences (IASBS)
Zanjan, Iran
dadashzadeh@iasbs.ac.ir

Abstract—Reliable diagnosis of brain tumors remains challenging due to low clinical incidence rates of such cases. However, this low rate is neglected in most of proposed methods. We propose a clinically inspired framework for anomaly-resilient tumor detection and classification. Detection leverages YOLOv8n fine-tuned on a realistically imbalanced dataset (1:9 tumor-to-normal ratio; 30,000 MRI slices from 81 patients). In addition, we propose a novel Patient-to-Patient (PTP) metric that evaluates diagnostic reliability at the patient level. Classification employs knowledge distillation: a Data Efficient Image Transformer (DeiT) student model is distilled from a ResNet152 teacher. The distilled ViT achieves an F1-score of 0.92 within 20 epochs, matching near-teacher performance (F1=0.97) with significantly reduced computational resources. This end-to-end framework demonstrates high robustness in clinically representative anomaly-distributed data, offering a viable tool that adheres to realistic situations in clinics.

Index Terms—Brain Tumor Diagnosis, Clinical Scenarios, Patient-to-Patient Metric, YOLOv8, Data Efficient Image Transformer, Vision Transformer.

I. INTRODUCTION

Brain tumors pose severe health risks where delayed diagnosis critically impacts survival outcomes [1]. Magnetic Resonance Imaging (MRI) serves as the clinical gold standard for detection due to its superior soft-tissue resolution [2], yet manual interpretation struggles with the extreme rarity of tumors (<0.1% incidence [3]) amidst vast normal data [4]. This *clinical imbalance*, compounded by high tumor heterogeneity [5], undermines traditional computer-aided diagnosis systems.

Existing deep learning approaches—including GAN-augmented CNNs [6], attention mechanisms [7], and Vision Transformers (ViTs) [8]—often rely on semi-balanced datasets misrepresenting real-world scarcity. While achieving high image-level accuracy (e.g., 98.7% for ensemble ViTs [9]),

they neglect patient-level diagnostic reliability and practical deployability in resource-constrained settings [8], [10].

To bridge this gap, we introduce an *anomaly-aware* framework comprising:

- 1) **Clinically representative data:** Curated NBML dataset (81 patients; 30,000 MRI slices) preprocessed to enforce 1:9 tumor-to-normal ratio both at slice and patient level.
- 2) **Patient-level evaluation:** Novel **PTP metric** assessing diagnostic reliability across full patient studies.
- 3) **Efficient two-stage architecture:**
 - *Detection:* YOLOv8n fine-tuned for robust localization in imbalanced data.
 - *Classification:* Knowledge distillation via DeiT [11], transferring ResNet152 insights to compact ViT.

Our approach optimizes both accuracy (PTP-F1=1.0; classification F1=0.92) and computational efficiency for clinical deployment.

Section II is a literature review on related work in this field. Section III describes the dataset used in this study. Section V presents the results we achieved, and Section VI concludes the article.

II. RELATED WORK

Recent hardware advances, particularly GPUs, have demonstrated deep learning as the dominant paradigm for brain tumor diagnosis [12], [13]. Representative works from key methodological approaches demonstrate both progress and persistent challenges:

Ahmad *et al.* [6] pioneered generative data augmentation using VAE-GAN hybrids, boosting ResNet50 accuracy to 96.25%. However, such methods incur prohibitive computational costs that limit clinical utility. Sharif *et al.* [10]

exemplified feature selection techniques with their EKbHFV-MGA framework, achieving 95% accuracy but introducing complexity that impedes cross-dataset generalization. Vision Transformer innovations are well-represented by Asiri *et al.* [8] (FT-ViT) and Tummala *et al.* [9] (ViT ensembles), reaching up to 98.7% accuracy at the cost of extreme computational demands. For detection tasks, Abdusalomov [14] demonstrated attention-enhanced YOLOv7 with CBAM/SPPF+ layers achieving 99.5% accuracy, though crucially evaluated on balanced datasets that misrepresent clinical reality.

While these representative works achieve high image-level accuracy, they collectively neglect three critical clinical requirements: 1) patient-level diagnostic reliability; 2) performance under true incidence rates ($<0.1\%$ tumors); and 3) computational constraints of medical environments. Our framework addresses these gaps through novel patient-centric evaluation (PTP metric) and resource-optimized architecture design.

III. DATA AND RESOURCES

A. NBML Dataset

The dataset from the National Brain Mapping Lab (NBML) which we used for detection includes MRI slices captured through T1-weighted, T2-weighted, and diffusion-weighted sequences, as well as other imaging modalities such as PET and CT scans. It is important to note that this dataset remains privately held, with all associated rights and credits attributed to the Iranian Brain Mapping Biobank (IBMB).

B. Kaggle Dataset

For tumor classification, we combined and preprocessed two public sources namely Kaggle Brain Tumor MRI Dataset (accessed on August 2023) and Figshare dataset [15].

Our custom augmentation module generated variations to increase sample diversity and it was partitioned into training, validation, and benchmark sets for rigorous evaluation.

C. Computational Resources

Experiments used an NVIDIA GTX 1650 GPU locally and Google Colab's T4 GPU. We employed PyTorch 2.0.1+cu117/Python 3.9.7, with ViT from Wang's GitHub [16] and TorchVision's ResNet152.

IV. PROPOSED METHOD

Accurate and realistic brain tumor diagnosis involves two distinct goals: 1) detecting tumors within a predominantly normal dataset, and 2) identifying unusual brain tissues and their types from unique characteristics in noisy scenes (e.g., shape and suspicious tissue placement).

The tumor detection, focuses on training a model that is resilient to *anomaly-distributed* populations and can accurately detect brain tumors in various imaging modalities.

The tumor classification, involves designing a custom DeiT model and training it to classify brain tumors in three classes of Meningioma, Pituitary, and Glioma.

A. Tumor detection

This phase utilizes the NBML dataset with 81 patients (30 tumor, 51 normal) to simulate clinical imbalance through specialized preprocessing.

1) **Rationale for Choosing YOLOv8:** We selected YOLOv8n for tumor detection based on three key advantages:

- *Performance in complex scenarios:* Architectural enhancements (advanced backbone/neck modules) improve detection in noisy medical images [17].
- *Generalization capability:* Effective transfer learning compensates for limited annotated data [18].
- *Computational efficiency:* Optimized for deployment in resource-constrained clinical environments.

The model was fine-tuned for our detection task and evaluated using both standard metrics and our novel PTP framework.

2) **Data Preprocessing:** The essence of our data preparation pipeline centers on the careful pre-processing of our data set to closely mirror real-world scenarios. In the context of brain tumors, the United States typically reports [19] incidence rate less than 0.1. Given the limitations stemming from our limited dataset for the detection phase and the absence of comprehensive external data sources, we exercised caution by adopting a conservative estimate of a 0.1 incidence rate.

3) **Realistic splitting:** To maintain clinically representative data distribution, we partitioned the dataset into training and testing sets while preserving our target 1:9 tumor-to-normal ratio. For the training set, we ensured nine randomly selected normal images were paired with each tumor image. This approach trains the model to recognize robust features across diverse patient scenarios rather than individual cases.

For the testing set, we selected 30 complete patient studies: 27 normal cases and 3 tumor cases (10% incidence), preserving all associated images per patient. This presented significant challenges due to:

- Variable image counts across patients
- Complex directory structures with modality-specific sub-folders (PET/CT/MRI types)
- Initial dataset imbalance versus target distribution
- Tumor-free slices in tumor patient folders

Here is our systematic approach:

- 1) DICOM to JPG conversion (540×540) using MicroDicom.
- 2) Patient directory compression to ZIP archives to:
 - Efficiently quantify total image volume.
 - Avoid recursive directory traversal of nested modality folders.
- 3) Testing set selection by ZIP size:
 - 27 normal patients: Smallest ZIPs.
 - 3 tumor patients: Smallest uncleaned ZIPs.
- 4) Training set construction:
 - $\sim 1.4k$ tumor-indicative images (cleaned cases).
 - 12,000 normal images (1:9 tumor-to-normal ratio).
- 5) Augmentation implementation:
 - Brightness adjustments,

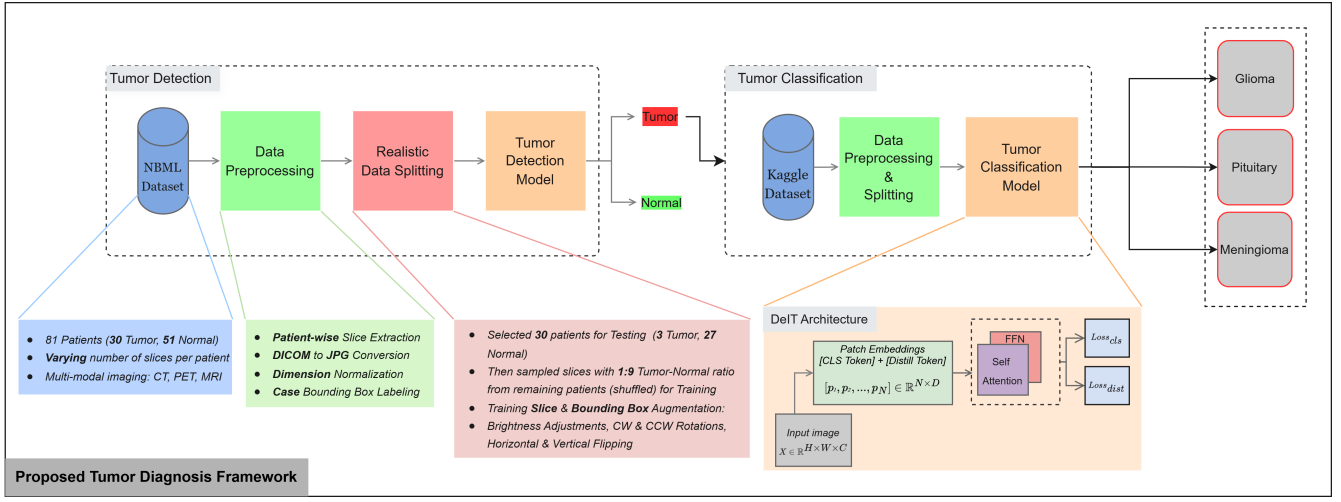


Fig. 1. Proposed Framework

- Vertical/horizontal flips,
- Bounding box-preserving rotations.

4) **Proposed Evaluation Metrics:** Standard image-level metrics were employed alongside our novel Patient-to-Patient (PTP) framework to evaluate model effectiveness. Precision, Recall, and F1-score are defined as:

$$Precision = TP / (TP + FP), \quad (1)$$

$$Recall = TP / (TP + FN), \quad (2)$$

$$F1 = 2 \times (Precision \times Recall) / (Precision + Recall) \quad (3)$$

where TP denotes True Positives, TN True Negatives, FP False Positives, and FN False Negatives.

To address clinical needs in imbalanced settings, we developed the PTP metric framework. This approach processes all images per patient directory, computes a Patient-Specific Tumor Threshold (PSTT) as:

$$PSTT = \frac{\# \text{ Tumor-indicative images}}{\# \text{ Total images}} \quad (4)$$

and classifies the case as tumor-positive if $PSTT > GTT$. Based on these definitions, four evaluation metrics are derived:

PTP-Accuracy measures overall patient classification correctness, calculated as the proportion of correctly classified patients.

PTP-Recall quantifies sensitivity for tumor patients, representing the fraction of actual tumor patients correctly identified.

PTP-Precision assesses positive predictive value by measuring the proportion of correctly identified tumor patients among all patients classified as tumor-positive.

PTP-F1 provides a balanced measure through the harmonic mean of PTP-Precision and PTP-Recall:

$$PTP-F1 = \frac{2 \times PTP-Precision \times PTP-Recall}{PTP-Precision + PTP-Recall} \quad (5)$$

This framework is exclusively deployed for tumor detection evaluation, while classification phase assessment utilizes standard accuracy metrics.

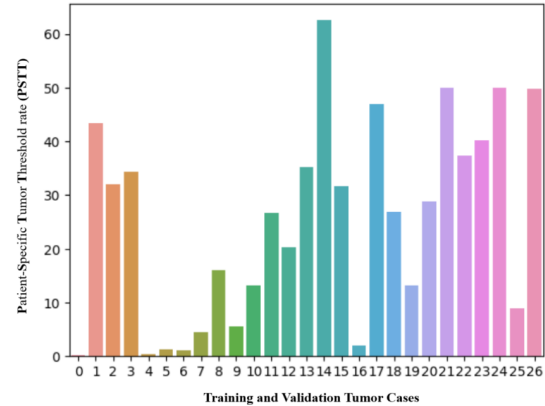


Fig. 2. PSTT, computed for each patient, represents the proportion of images depicting tumors within the entire image set for that patient.

5) **General Tumor Threshold:** The General Tumor Threshold (GTT) is the minimum percentage of tumor-indicative images required within a patient's complete scan set to classify them as tumor-positive. We determined this critical threshold through careful analysis of our training and validation data.

We processed all the patients scans within the training and validation sets through our detection model and calculated the value of GTT for each patient. After an exploratory analysis of the PSTT (Fig 2) values among the both Normal and Tumor cases, we estimated the value of the GTT to be at least 0.04%. This value is calculated from the average of the first quartile and the median values of tumor-indicative distribution.

B. Tumor classification

In this step, We employed Knowledge Distillation (KD) [20] to train a lightweight Vision Transformer (ViT) using our classification dataset, with ResNet152 as the teacher model. KD enables the student model (ViT) to learn from the teacher’s complete output distribution (soft labels), not just final predictions. This compresses knowledge from large models into efficient architectures while boosting performance.

1) **Justification for Choosing DeiT**: In this study, the DeiT [11] model was selected as the backbone for the classification phase due to several important factors that make it particularly suitable for our use case:

- 1) *Data Efficiency*: DeiT excels well with limited medical imaging data
- 2) *Performance Balance*: It maintains high accuracy while reducing model size
- 3) *Computational Advantage*: Distillation from ResNet152 (Strong Teacher) enables:
 - Faster training than standard ViTs
 - Lower inference costs
 - Near-teacher performance (least compromise)

C. Vision Transformer

Our pipeline employs the Vision Transformer (ViT) [21], adapting language processing principles to images. Key processing stages:

- *Patch creation*: Splits input ($\mathbb{R}^{H \times W \times C}$) into N patches of size $P \times P \times C$ where $N = HW/P^2$
- *Embedding*: Linear projection with added positional encodings
- *Classification token*: Learnable [CLS] embedding for final prediction
- *Encoder*: Transformer blocks alternating multi-head self-attention and MLP operations

This architecture provides global context modeling [22], crucial for tumor classification [8].

V. RESULTS

This section elaborates on the experiments and the results we achieved from deploying the proposed pipeline.

A. Tumor Detection Results

The initial step in this phase was data pre-processing. After conducting a comprehensive data preparation, we loaded the YOLOv8n pre-trained weights, tailored its hyper-parameters and fine-tuned it on our detection dataset.

Due to computational constraints, we selected YOLOv8n (Nano) and used larger batch sizes to accelerate training. While advanced versions (YOLOv8m/L) may improve results, they require significantly more resources and longer training times.

We trained the mentioned model for 40 epochs, and the evaluation results indicated (Table II) that the model is highly accurate in detecting tumor-confiscated images, and despite being agile and super lightweight with only 3.2M parameters, it does have a reliable performance.

TABLE I
YOLOV8N MODEL CONFIGURATION

Opt	Sched	lr0	lrf	AMP	Epochs
SGD	CosLR	0.01	0.00001	False	40

Opt: Optimizer, Sched: Scheduler, lr0: Initial learning rate, lrf: Final learning rate, AMP: Automatic Mixed Precision.

TABLE II
YOLOV8N MODEL EVALUATION RESULTS

Class	Precision	Recall	F1	Support
Tumor	0.99	0.96	0.97	1905
Normal	0.99	0.99	0.99	20750
AVG	0.99	0.975	0.98	22655

As for the patient-level assessment, the detection model achieved perfect scores for both tumor and normal cases, with an PTP F1-score of 1.0 across the testing population. This highlights the model’s ability to generalize well to real-world clinical scenarios, where detecting tumors in anomaly-distributed data is crucial.

Furthermore, the performance of the detection model, as demonstrated in Fig. 3, provides a clear indication of its robustness. Throughout training, the validation metrics show consistent improvement, while the training loss decreases steadily. This parallel progression between training and validation suggests a well-balanced model that is neither underfitting nor overfitting. Overfitting manifests as a divergence between training and validation results—where training loss decreases but validation performance plateaus or worsens.

B. Tumor Classification Results

Our classification phase employed Knowledge Distillation (KD) with DeiT architecture. We constructed an augmented dataset from the Figshare source using our custom augmentation module, then fine-tuned the ResNet152 teacher model to leverage its robust feature extraction capabilities. During distillation, ResNet152 transferred rich feature representations to the DeiT student model, enabling efficient training from scratch.

We proceeded to tune the hyperparameters of the DeiT model by iteratively exploring 14 different architectural variations to find the optimal settings. The specifics of these experiments are detailed in Table III.

Then we evaluated the optimal DeiT configuration on 461 test images across three tumor classes and achieved:

- **Pituitary**: F1-Score = 0.97
- **Glioma**: F1-Score = 0.93
- **Meningioma**: F1-Score = 0.82

The results in Table IV indicates that the student model despite having access to *relatively small* size dataset and being trained for *limited number* of epochs, is still effective in learning the distinguishing features of each tumor type. Also the Meningioma class seems to have a data integrity problem and the original data sources seems to lack the data diversity required for training a reliable model on them. This issue

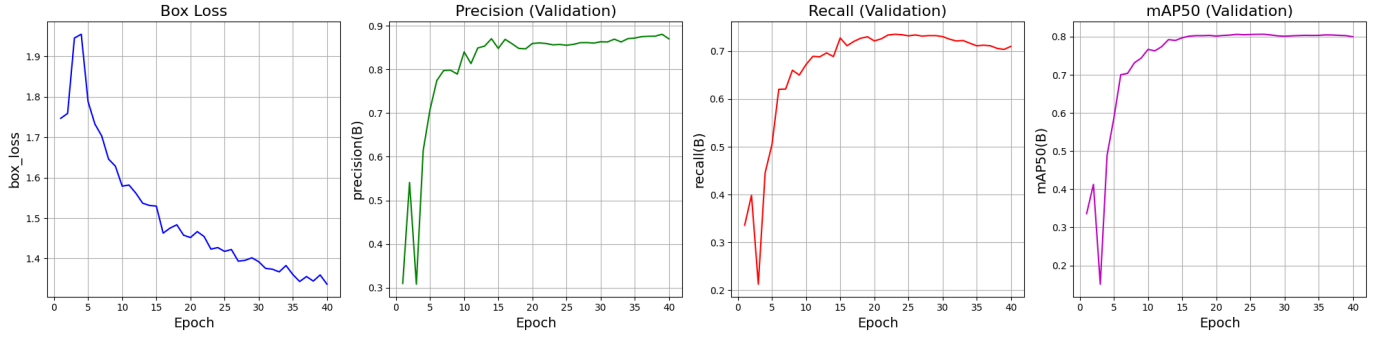


Fig. 3. Validation Performance Metrics and Training Loss Over Epochs for the YOLOv8n Detection Model.

TABLE III
DEiT HYPER-PARAMETERS TUNING EXPERIMENTS

No.	Hard Distillation	Temperature	Depth	Patch Size	Dimension	Attention Head	MLP Dim	Val-Accuracy
1	False (Default)	2 (Default)	4 (Default)	24 (Default)	256 (Default)	16 (Default)	128 (Default)	81.91
2	True	2 (Default)	4 (Default)	24 (Default)	256 (Default)	16 (Default)	128 (Default)	84.74
3	True	1	4 (Default)	24 (Default)	256 (Default)	16 (Default)	128 (Default)	83.22
4	True	9	4 (Default)	24 (Default)	256 (Default)	16 (Default)	128 (Default)	81.69
5	True	3	6	24 (Default)	256 (Default)	16 (Default)	128 (Default)	82.35
6	True	3	2	32	256 (Default)	16 (Default)	128 (Default)	85.40
7	True	3	2	24	256 (Default)	16 (Default)	128 (Default)	86.05
8	True	3	2	24	1024	16 (Default)	128 (Default)	68.19
9	True	3	2	24	128	16 (Default)	128 (Default)	85.40
10	True	3	2	24	512	16 (Default)	128 (Default)	74.29
11	True	3	2	24	128	64	128 (Default)	88.67
12	True	3	2	24	128	64	256	88.45
13	True	3	2	24	128	64	2048	87.58
14	True	3	2	24	128	64	512	89.76

could be solved by SMOTE or weighted loss functions and perhaps data augmentation, however the main objective here was to prove that even in these scenarios the student model still performs pretty good.

As indicated in Table IV, student model achieved a competitive F1-Score of 0.92 compared to the ResNet152 teacher's 0.97 (Table V). This performance difference primarily stems from the teacher's training on heavily augmented data, which enhanced feature generalization but required substantial computational resources. In contrast, the DeiT student was trained for only 20 epochs without augmentation using minimal resources.

TABLE IV
DISTILLED STUDENT CLASSIFIER TEST RESULTS

Tumor Class	Precision	Recall	F1	Support
Meningioma	0.82	0.82	0.82	107
Glioma	0.95	0.92	0.93	214
Pituitary	0.95	0.99	0.97	140
Weighted AVG	0.92	0.92	0.92	461

Crucially, both models were evaluated on an identical holdout test set (15% benchmark allocation), preventing data leakage while ensuring fair comparison. This confirms DeiT's efficiency for clinical deployment.

TABLE V
TEACHER CLASSIFIER TEST RESULTS

Tumor Class	Precision	Recall	F1	Support
Meningioma	0.92	0.91	0.91	107
Glioma	0.99	0.97	0.98	214
Pituitary	0.94	0.97	0.96	140
Weighted AVG	0.97	0.97	0.97	461

VI. CONCLUSION

This work presented a novel framework for the detection and classification of brain tumors. To realistically simulate the low incidence rate brain tumor clinical diagnosis scenarios, an extensive, meticulous data preprocessing steps were applied.

As for the detection, we introduced a new set of performance metrics namely PTP-metrics with a focus on capturing the performance in clinical scenarios. Further, we trained YOLOv8 for a few epochs and achieved near to perfect results, indicating a anomaly robust performance.

Furthermore, in the classification we distilled an student model from ResNet152 teacher using DeiT architecture and achieved comparative performance.

This work is the first in literature that introduced a close to clinical framework to capture the tumor detection performance at patient level scope rather than individual slices, hence further refinement of the GTT and the extension of PTP-

like metrics to classification task remains an area for potential future investigation.

Code Availability

The implementation code is available at:
https://github.com/MHosseinHashemi/NBML_BrTD

REFERENCES

- [1] G. S. Tandel, M. Biswas, O. G. Kakde, A. Tiwari, H. S. Suri, M. Turk, J. R. Laird, C. K. Asare, A. A. Ankrah, N. Khanna *et al.*, “A review on a deep learning perspective in brain cancer classification,” *Cancers*, vol. 11, no. 1, p. 111, 2019.
- [2] R. Augustine, A. Al Mamun, A. Hasan, S. A. Salam, R. Chandrasekaran, R. Ahmed, and A. S. Thakor, “Imaging cancer cells with nanostructures: Prospects of nanotechnology driven non-invasive cancer diagnosis,” *Advances in Colloid and Interface Science*, vol. 294, p. 102457, 2021.
- [3] “Brain Tumors and Brain Cancer,” 2023, [Online; accessed 31. Aug. 2023]. [Online]. Available: <https://www.hopkinsmedicine.org/health/conditions-and-diseases/brain-tumor>
- [4] K. Popuri, D. Cobzas, A. Murtha, and M. Jägersand, “3d variational brain tumor segmentation using dirichlet priors on a clustered feature set,” *International journal of computer assisted radiology and surgery*, vol. 7, pp. 493–506, 2012.
- [5] J. Kang, Z. Ullah, and J. Gwak, “Mri-based brain tumor classification using ensemble of deep features and machine learning classifiers,” *Sensors*, vol. 21, no. 6, p. 2222, 2021.
- [6] B. Ahmad, J. Sun, Q. You, V. Palade, and Z. Mao, “Brain tumor classification using a combination of variational autoencoders and generative adversarial networks,” *Biomedicines*, vol. 10, no. 2, p. 223, 2022.
- [7] A. B. Abdusalomov, M. Mukhiddinov, and T. K. Whangbo, “Brain tumor detection based on deep learning approaches and magnetic resonance imaging,” *Cancers*, vol. 15, no. 16, p. 4172, 2023.
- [8] A. A. Asiri, A. Shaf, T. Ali, U. Shakeel, M. Irfan, K. M. Mehdar, H. T. Halawani, A. H. Alghamdi, A. F. A. Alshamrani, and S. M. Alqhtani, “Exploring the power of deep learning: Fine-tuned vision transformer for accurate and efficient brain tumor detection in mri scans,” *Diagnostics*, vol. 13, no. 12, p. 2094, 2023.
- [9] S. Tummala, S. Kadry, S. A. C. Bukhari, and H. T. Rauf, “Classification of brain tumor from magnetic resonance imaging using vision transformers ensembling,” *Current Oncology*, vol. 29, no. 10, pp. 7498–7511, 2022.
- [10] M. I. Sharif, M. A. Khan, M. Alhussein, K. Aurangzeb, and M. Raza, “A decision support system for multimodal brain tumor classification using deep learning,” *Complex & Intelligent Systems*, pp. 1–14, 2021.
- [11] H. Touvron, M. Cord, M. Douze, F. Massa, A. Sablayrolles, and H. Jégou, “Training data-efficient image transformers & distillation through attention,” in *International conference on machine learning*. PMLR, 2021, pp. 10 347–10 357.
- [12] N. S. Shaik and T. K. Cherukuri, “Multi-level attention network: application to brain tumor classification,” *Signal, Image and Video Processing*, vol. 16, no. 3, pp. 817–824, 2022.
- [13] M. F. Alanazi, M. U. Ali, S. J. Hussain, A. Zafar, M. Mohatram, M. Irfan, R. AlRuwaiti, M. Alruwaiti, N. H. Ali, and A. M. Albarrak, “Brain tumor/mass classification framework using magnetic-resonance-imaging-based isolated and developed transfer deep-learning model,” *Sensors*, vol. 22, no. 1, p. 372, 2022.
- [14] A. B. Abdusalomov, M. Mukhiddinov, and T. K. Whangbo, “Brain Tumor Detection Based on Deep Learning Approaches and Magnetic Resonance Imaging,” *Cancers*, vol. 15, no. 16, August 2023.
- [15] J. Cheng, “Brain tumor dataset,” *figshare. Dataset*, vol. 1512427, no. 5, 2017.
- [16] “vit-pytorch,” 2023, [Online; accessed 31. Aug. 2023]. [Online]. Available: <https://github.com/lucidrains/vit-pytorch>
- [17] J. Solawetz, “What is YOLOv8? The Ultimate Guide,” *Roboflow Blog*, December 2023. [Online]. Available: <https://blog.roboflow.com/whats-new-in-yolov8>
- [18] M. G. Ragab, S. J. Abdulkadir, A. Muneer, A. Alqushaibi, E. H. Sumiea, R. Qureshi, S. M. Al-Selwi, and H. Alhussian, “A Comprehensive Systematic Review of YOLO for Medical Object Detection (2018 to 2023),” *IEEE Access*, vol. 12, pp. 57 815–57 836, Apr. 2024.
- [19] “Cancer of the Brain and Other Nervous System - Cancer Stat Facts,” 2023, [Online; accessed 31. Aug. 2023]. [Online]. Available: <https://seer.cancer.gov/statfacts/html/brain.html>
- [20] G. Hinton, O. Vinyals, and J. Dean, “Distilling the knowledge in a neural network,” *arXiv preprint arXiv:1503.02531*, 2015.
- [21] A. Dosovitskiy, L. Beyer, A. Kolesnikov, D. Weissenborn, X. Zhai, T. Unterthiner, M. Dehghani, M. Minderer, G. Heigold, S. Gelly *et al.*, “An image is worth 16x16 words: Transformers for image recognition at scale,” *arXiv preprint arXiv:2010.11929*, 2020.
- [22] A. Vaswani, N. Shazeer, N. Parmar, J. Uszkoreit, L. Jones, A. N. Gomez, Ł. Kaiser, and I. Polosukhin, “Attention is all you need,” *Advances in neural information processing systems*, vol. 30, 2017.